Title	Dipole resonances in light neutron-rich nuclei studied with time-dependent calculations of antisymmetrized molecular dynamics
Author(s)	Kanada-En'yo, Y; Kimura, M
Citation	PHYSICAL REVIEW C (2005), 72(6)
Issue Date	2005-12
URL	http://hdl.handle.net/2433/50444
Right	Copyright 2005 American Physical Society
Type	Journal Article
Textversion	publisher

Dipole resonances in light neutron-rich nuclei studied with time-dependent calculations of antisymmetrized molecular dynamics

Y. Kanada-En'yo and M. Kimura
Yukawa Institute for Theoretical Physics, Kyoto University, Kyoto 606-8502, Japan
(Received 22 July 2005; published 6 December 2005)

To study isovector dipole responses of neutron-rich nuclei, we applied a time-dependent method of antisymmetrized molecular dynamics. The dipole resonances in Be, B, and C isotopes were investigated. In ^{10}Be, ^{15}B, and ^{16}C, collective modes of the vibration between a core and valence neutrons cause soft resonances at the excitation energy $E_x = 10$–15 MeV below the giant dipole resonance (GDR). In ^{16}C, we found that a remarkable peak at $E_x = 14$ MeV corresponds to the coherent motion of four valence neutrons against a ^{12}C core, whereas the GDR arises in the $E_x > 20$ MeV region because of vibration within the core. In ^{17}B and ^{18}C, the dipole strengths in the low-energy region decline compared with those in ^{15}B and ^{16}C. We also discuss the energy-weighted sum rule for the $E1$ transitions.

DOI: 10.1103/PhysRevC.72.064301 PACS number(s): 21.60.−n, 24.30.Cz, 21.10.Re

I. INTRODUCTION

In neutron-rich nuclei, there appear exotic phenomena that are very different from those in stable nuclei because of the excess neutrons. Some of these phenomena are concerned with differences between proton and neutron densities. Neutron halo and skin structures are typical examples. Other related subjects are deformations of proton and neutron densities. For example, the difference of the deformations between proton and neutron densities were theoretically suggested in Be, B, and C isotopes [1–3]. These phenomena imply that the structure of nuclei far from the β-stability line often contradicts the usual understanding for stable nuclei in which the proton and neutron densities are consistent with each other in a nucleus. They may also lead to exotic phenomena in excitations and reactions. One of the current issues is the dipole excitations in neutron-rich nuclei [4–21]. In a system with different proton and neutron densities, because the energy of isovector-dipole excitations may become low, soft resonances below the giant dipole resonance (GDR) are naturally expected. Their collectivity and the contributions of the excess neutrons have attracted interest. In fact, the features of dipole transitions in neutron-rich O isotopes have been studied experimentally [20] and theoretically [11,13,16], and the dipole strengths have been found to be different from those in the stable nucleus, ^{16}O, especially in the low-energy region below the GDR. The dipole excitations have been studied also in C isotopes by Suzuki *et al.* with shell-model calculations [17]; they suggested that coherent neutron transitions may enhance the strengths at excitation energy $E_x = 10$–15 MeV.

Our present interest is in the isovector-dipole excitations in the light neutron-rich nuclei and in the effect of the ground-state properties such as deformations. A method of antisymmetrized molecular dynamics (AMD) [1] is one of powerful approaches for nuclear structure study. The method is superior, especially in the description of the cluster aspect, which is important in light unstable nuclei as well as in light stable nuclei [22]. In the systematic studies of Be, B, and C isotopes with the AMD method, a variety of structures such as neutron skins and deformations has been suggested in those nuclei, and some phenomena have been discussed in relation to the cluster aspect [1,22]. The experimental data for various properties of the neutron-rich Be, B, and C isotopes are well reproduced by the AMD calculations. We should stress that the AMD calculations agree well with the experimental data of quadrupole moments and $E2$ strengths in neutron-rich B and C, which cannot be reproduced by the shell-model calculations without using system-dependent effective charges. For the study of dipole excitations in the AMD framework, we apply a time-dependent method and calculate dipole strengths in a similar way to the time-dependent Hartree-Fock (TDHF) method. The point is that we are able to study dipole resonances within the framework that can describe the cluster aspect. One of the advantages of the time-dependent AMD is that we can link the excitations with collective modes such as core vibration, core-neutron motion, and intercluster motion which should be important for our understanding of the role of excess neutrons in dipole resonances in neutron-rich systems. Another advantage is that the present AMD model is free from the spurious center-of-mass motion in the calculations of the dipole strengths.

The time-dependent method of AMD was proposed and applied to heavy-ion reactions by Ono *et al.* in 1992 [23,24], which is earlier than the application of the AMD to nuclear structure studies. However, the time-dependent AMD calculations have not yet been performed for collective motion on the static solution. In this paper, we formulate a method based on the time-dependent AMD for the study of the $E1$ response in analogy to the TDHF. To see its validity, we first apply it to ^{12}C and ^{18}O and show a comparison of the results, the experimental data, and other theoretical calculations. Then we apply this method to Be, B, and C isotopes and discuss the properties of dipole strengths in the neutron-rich nuclei. We try to see how the dipole strength distribution is influenced by structures such as the deformations, the neutron skin, and existence of core and clusters.

This paper is organized as follows. In the next section, we explain the formulation of the present method for the $E1$ response, which is based on the time-dependent AMD. Adopted effective nuclear forces are described in Sec. III.

In Sec. IV, we show the results of ^{12}C and ^{18}O and the comparison with experimental data and also the dipole transitions in Be, B, and C isotopes. Discussions of the $E1$ excitations in neutron-rich Be, B, and C isotopes are given in Sec. V. Finally, in Sec. VI we give a summary.

II. FORMULATION

We explain the formulation of the time-dependent version of AMD for calculations of isovector-dipole excitations. By simulating the time evolution of the collective motion on the static solution with the time-dependent AMD, we can calculate the response of a nucleus to external dipole fields and obtain the dipole strengths in the similar way to TDHF approaches.

The time-dependent method in the AMD framework is described in Refs. [23,24], in which the method was applied to heavy-ion collisions. Concerning nuclear structure study by AMD methods, Refs. [22,25] review the static version of AMD and its extended versions.

A. Wave function

The wave function for an A-nucleon system (A is a mass number) is given by a single Slater determinant of Gaussian wave packets as

$$\Phi = \frac{1}{\sqrt{A!}}\mathcal{A}\{\varphi_1, \varphi_2, \ldots, \varphi_A\}, \tag{1}$$

where the ith single-particle wave function is written as

$$\varphi_i = \varphi_{\mathbf{Z}_i}\chi_i\tau_i, \tag{2}$$

$$\varphi_{\mathbf{Z}_i}(\mathbf{r}_j) = \left(\frac{2\nu}{\pi}\right)^{3/4}\exp\left[-\nu\left(\mathbf{r}_j - \frac{\mathbf{Z}_i}{\sqrt{\nu}}\right)^2\right], \tag{3}$$

$$\chi_i = \left(\frac{1}{2}+\xi_i\right)\chi_\uparrow + \left(\frac{1}{2}-\xi_i\right)\chi_\downarrow. \tag{4}$$

Here, the spatial part of the ith single-particle wave function is given by a located Gaussian wave packet, whose center is represented by the complex parameter $\mathbf{Z}_i$. The parameter ξ_i indicates the intrinsic-spin orientation, and the isospin function τ_i is up (proton) or down (neutron).

In this work, the orientation of the intrinsic spin is fixed to be up or down as $\xi_i = \{1/2, -1/2\}$ for simplicity. In this AMD wave function, all the centers of Gaussian wave packets for A nucleons are independent variational parameters, and a set of parameters $\mathbf{Z} \equiv \{\mathbf{Z}_1, \mathbf{Z}_2, \cdots, \mathbf{Z}_A\}$ specifies the total wave function $\Phi(\mathbf{Z})$ of the state. This is the simplest version of the AMD wave function, and parity and angular-momentum projections are not performed in this work.

B. Equation of motion

In the time-dependent version of AMD, $\mathbf{Z}$ are considered to be time-dependent parameters, as explained in [24]. The time evolution of the system is determined by the time-dependent variational principle,

$$\delta\int_{t_1}^{t_2} dt\,\frac{\langle\Phi(\mathbf{Z})|i\hbar\frac{d}{dt} - H|\Phi(\mathbf{Z})\rangle}{\langle\Phi(\mathbf{Z})|\Phi(\mathbf{Z})\rangle} = 0. \tag{5}$$

This leads to the equations of motion with respect to $\mathbf{Z}$,

$$i\hbar\sum_{j,\tau} C_{i\sigma,j\tau}\dot{Z}_{j\tau} = \frac{\partial\mathcal{H}}{\partial Z^*_{i\sigma}} \quad \text{and} \quad \text{c.c.}, \tag{6}$$

where $\sigma, \tau = x, y, z$, and $\mathcal{H}$ is the expectation value of the Hamiltonian H:

$$\mathcal{H}(\mathbf{Z}, \mathbf{Z}^*) = \frac{\langle\Phi(\mathbf{Z})|H|\Phi(\mathbf{Z})\rangle}{\langle\Phi(\mathbf{Z})|\Phi(\mathbf{Z})\rangle}. \tag{7}$$

$$C_{i\sigma,j\tau} \equiv \frac{\partial^2}{\partial Z^*_{i\sigma}\partial Z_{j\tau}}\ln\langle\Phi(\mathbf{Z})|\Phi(\mathbf{Z})\rangle \tag{8}$$

is a positive-definite Hermitian matrix. Equations (6)–(8) are derived in general from the time-dependent variational principle for a given wave function parametrized by complex variational parameters. In the case of the AMD framework, the time evolution of a system is described by the motion of the centers of Gaussian wave packets.

Although a stochastic collision process has been introduced in studies of heavy-ion collisions [24], we do not put it in the present framework.

C. Response to dipole fields

To calculate the response to external fields, we first solve the static problem to obtain the optimum solution Ψ^0 for the ground state. We perform an energy variation of the AMD wave function with respect to the variational parameter $\mathbf{Z}$ by using the frictional cooling method (an imaginary-time method) [22–24]. After the energy variation, we obtain the optimum parameter set $\mathbf{Z}^0$, which gives the energy minimum state $\Psi^0 = \Phi(\mathbf{Z}^0)$ in the AMD model space. Then we boost the Ψ^0 instantaneously at $t = 0$ by imposing an external perturbative field, $V_{\text{ext}}(\mathbf{r}, t) = \epsilon F(\mathbf{r})\delta(t)$, where ϵ is an arbitrary small number. This results in an initial state of the time-dependent calculation:

$$\Psi(t = 0+) = e^{-i\epsilon F}\Psi^0 = e^{-i\epsilon F}\Phi(\mathbf{Z}^0). \tag{9}$$

In the calculation of $E1$ resonances, the external field is chosen to be the dipole field:

$$F(\mathbf{r}) = \mathcal{M}(E1, \mu) = \sum_i^A e^{\text{rec}} r_i Y_{1\mu}(\hat{\mathbf{r}}_\mathbf{i}), \tag{10}$$

where e^{rec} is the $E1$ recoil charge, Ne/A for protons and $-Ze/A$ for neutrons. We write the initial state $\Psi(t = 0+)$ with a single AMD wave function $\Phi[\mathbf{Z}(t = 0+)]$ by simply transforming the parameters $\mathbf{Z}^0 = \{\mathbf{Z}^0_1, \mathbf{Z}^0_2, \cdots, \mathbf{Z}^0_A\}$ as follows:

$$\mathbf{Z}_i(t = 0+) = \mathbf{Z}^0_i - \frac{\epsilon e^{\text{rec}}\mathbf{e}_\mu}{2\sqrt{\nu}}i, \tag{11}$$

where $\mathbf{e}_\mu$ is the unit vector. Although an extra normalization factor of the wave function arises from this transformation, it has no effect on physical quantities because the AMD framework is always based on the normalized wave functions.

By using the equation of motion [Eq. (6)], we can calculate the time evolution of the system $\Psi(t) = \Phi[\mathbf{Z}(t)]$ from the

initial state $\Psi(t=0+)=\Phi[\mathbf{Z}(t=0+)]$ following the time-dependent AMD. The transition strength is obtained by a Fourier transform of the expectation value of $\mathcal{M}(E1,\mu)$: as follows,

$$\frac{dB(\omega;E1,\mu)}{d\omega} \equiv \sum_n |\langle n|\mathcal{M}(E1,\mu)|0\rangle|^2\delta(\omega-\omega_n) = -\frac{1}{\pi\epsilon}\mathrm{Im}\int_0^\infty dt\langle\Psi(t)| \times \mathcal{M}(E1,\mu)|\Psi(t)\rangle e^{i\omega t}, \quad (12)$$

where $|0\rangle$ is the ground state and $|n\rangle$ is the excited state with the excitation energy $\hbar\omega_n$. In a deformed nucleus, Eq. (12) gives the $E1$ transition strengths in the intrinsic state because the total angular-momentum projection is not performed. Assuming the strong coupling scheme, we calculate the $B(E1)$ in the laboratory frame by summing the intrinsic $E1$ strengths:

$$\frac{dB(\omega;E1)}{d\omega} = \sum_{K=0,\pm1}\frac{dB(\omega;E1,K)}{d\omega}. \quad (13)$$

In the practical calculation, we impose the $E1$ field with respect to each direction, x, y, and z, independently, and sum up the strengths instead of the sum of $K=0,\pm1$. Because the center-of-mass motion is constant and can be exactly separated from $\Psi(t)$, the present model is free from the spurious center-of-mass motion in the calculations of the dipole strengths. In the present framework, $dB(\omega;E1)/d\omega$ consists of discrete peaks in principle, because the present AMD is a bound-state approximation and continuum states are not taken into account. We introduce a smoothing parameter Γ, add an imaginary part $i\Gamma/2$ to the real excitation energy E_x as $\hbar\omega = E_x + i\Gamma/2$, and calculate the $B(E1)$ with Eq. (12) by performing the integral up to finite time. This smoothing can be considered as simulating the escape and the spreading widths of the resonances.

The photonuclear cross section $\sigma(\omega)$ is related to the transition strength $B(\omega;E1)$ as

$$\sigma(\omega) = \frac{16\pi^3}{9\hbar c}\hbar\omega\frac{dB(\omega;E1)}{d\omega}. \quad (14)$$

III. EFFECTIVE NUCLEAR INTERACTIONS

We use an effective nuclear interaction that consists of the central force, the spin-orbit force, and the Coulomb force. In the present work, we adopt the MV1 force [26] as the central force. This force contains a zero-range three-body force in addition to the finite-range two-body interaction:

$$V^{\mathrm{MV1}} = \sum_{i<j}V^{(2)} + \sum_{i<j<k}V^{(3)}, \quad (15)$$

$$V^{(2)} = (w + bP_\sigma - hP_\tau - mP_\sigma P_\tau) \times \left[V_1\exp\left(-\frac{r_{ij}^2}{a_1^2}\right) + V_2\exp\left(-\frac{r_{ij}^2}{a_2^2}\right)\right], \quad (16)$$

$$V^{(3)} = t_3\delta(\mathbf{r}_i-\mathbf{r}_j)\delta(\mathbf{r}_j-\mathbf{r}_k), \quad (17)$$

where P_σ and P_τ denote the spin and the isospin exchange operators, respectively. The two-body part contains Wigner ($w=1-m$), Bartlett (b), Heisenberg (h), and Majorana (m) terms. Concerning the spin-orbit force, the same range parameters as those of the G3RS force [27] are adopted. Coulomb force is approximated by the sum of seven Gaussians.

In this work, we use the same interaction parameters as those used in Ref. [1] except for ^{18}O; namely, we use case 3 of MV1 force and choose the Bartlett, Heisenberg, and Majorana parameters as $b=h=0$ and $m=0.576$, respectively. The strength of the spin-orbit force is chosen as $u_{\mathrm{I}} = -u_{\mathrm{II}} \equiv u_{\mathrm{ls}} =$ 900 MeV. For ^{18}O, we cannot obtain a stable solution of the AMD wave function without parity projection in the case of the parameter $m=0.576$ because of a problem of the numerical calculation. It is because the Gaussian centers $\mathbf{Z}_i$ gather to the origin and the norm of the AMD wave function becomes almost zero in the energy variation. To avoid this problem, we use a slightly large Majorana parameter, $m=0.62$ instead of $m=0.576$. We note that the properties of the ground state are not qualitatively unchanged in the parameter range $m=$ 0.576–0.63 in most nuclei [22].

IV. RESULTS

We apply the present method of AMD to dipole excitations in ^{8,10,14}Be, ^{11,15,17}B, ^{12,16,18,20}C, and ^{18}O. In the present AMD method without parity and spin projections, we cannot obtain static solutions for the $N=8$ isotones by the cooling method because of the divergence of the inverse norm of the wave function, because a system with $N=8$ favors the p-shell closed state, which is written by the AMD wave function with the zero limit of Gaussian centers ($\mathbf{Z}$) for all neutrons.

A. Properties of ground states

The wave functions of the ground states (Ψ^0) are obtained by the energy variation for the AMD wave function without spin-parity projections. The width parameter ν is fixed and chosen to be an optimum value for each nucleus to give the minimum energy of the ground state in most cases. For ^{15}B, ^{16}C, ^{18}C, and ^{18}O, we use slightly larger width parameters than the optimum values to avoid the numerical problem in the norm of the wave function. The adopted ν values are listed in Table I.

TABLE I. The adopted width parameters(ν) of the AMD wave functions.

Isotope	^{8}Be	^{10}Be	^{14}Be	^{11}B	^{15}B	^{17}B	^{12}C	^{16}C	^{18}C	^{20}C	^{18}O
ν (fm^{-2})	0.200	0.180	0.175	0.175	0.180	0.160	0.180	0.180	0.175	0.165	0.170

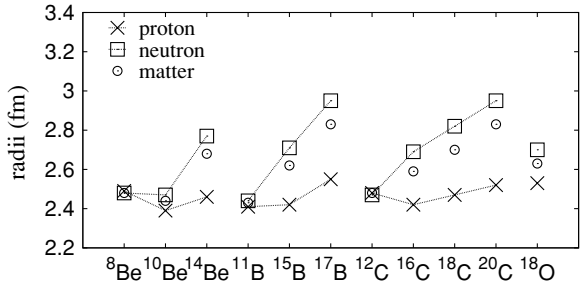

FIG. 1. The root-mean-square radii of the ground states obtained by the AMD calculation. The radii for the proton (neutron) density distributions of the ground state, Ψ^0, are plotted by crosses (squares). The circles indicate the nuclear matter radii.

As suggested in Refs. [1–3,22], the shape of the proton and neutron density distribution rapidly changes with the variation of the proton and neutron numbers. The root-mean-square radii for the ground states (Ψ^0) are shown in Fig. 1. In each series of isotopes, the neutron radius is enhanced in the neutron-rich nuclei with the increase of neutron number. In Fig. 2, we show the deformation parameters (β, γ) for proton and neutron densities. The results are qualitatively the same as the previous results obtained by the simple AMD calculations [2,3]. In some nuclei, the difference of the shape between protons and neutrons is found in the γ parameter as well as the β values. The discrepancy of γ between protons and neutrons is remarkable in ^{10}Be and ^{16}C. Namely, the opposite deformation between proton and neutron densities appears in these nuclei, as discussed in Refs. [2,3].

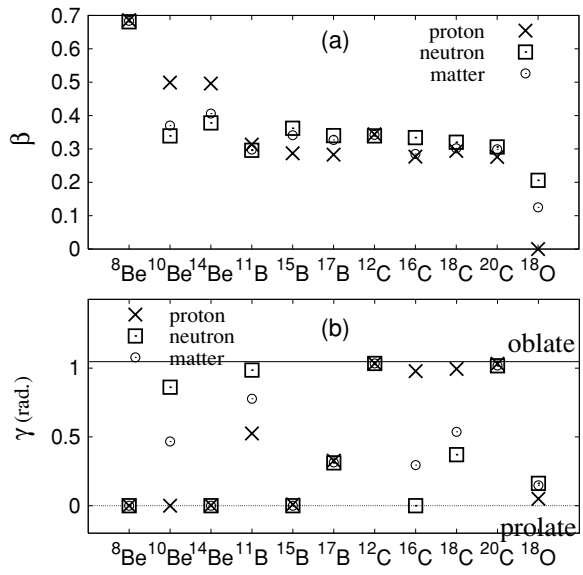

FIG. 2. The deformations of the ground states calculated by AMD. The deformation parameters (a) β and (b) γ for the proton (neutron) density distributions in Ψ^0 are plotted by crosses (squares). Circles indicate the deformations of nuclear matter density.

B. Energy-weighted sum rule

The energy-weighted sum rule (EWSR) for isovector-dipole resonances is given by

$$S(E1) = \int \hbar\omega \frac{dB(\omega; E1)}{d\omega} d\omega. \tag{18}$$

If the interaction commutes with the $E1$ operator, $S(E1)$ is identical to the classical Thomas-Reiche-Kuhn (TRK) sum rule:

$$S(\mathrm{TRK}) = \frac{9e^2}{8\pi M}\frac{NZ}{A}, \tag{19}$$

where M is the nucleon mass. Because of the contributions of exchange terms and momentum-dependent terms, the interaction is usually incommutable with the $E1$ operator and $S(E1)$ is enhanced compared with S(TRK). Following the method explained in Ref. [28], we can calculate the EWSR with the initial-state expectation value of the double commutator of the Hamiltonian with the dipole operator F:

$$S(E1) = \tfrac{1}{2}\langle\Psi^0|[F,[H,F]]|\Psi^0\rangle. \tag{20}$$

We estimate the enhancement factor, $\kappa = S(E1)/S(\mathrm{TRK}) - 1$, for the present interaction by neglecting the contribution of the spin-orbit force. The incommutable terms in the present interaction come from Heisenberg and Majorana exchange terms in the two-body central force $V^{(2)}$. If we write the two-body force as $V^{(2)} = v(r_{ij}) + v^\tau(r_{ij})\boldsymbol{\tau}_i \cdot \boldsymbol{\tau}_j$ [$\boldsymbol{\tau}$ is the isospin SU(2) generator], the enhancement $\Delta S(E1) = S(E1) - S(\mathrm{TRK})$ is given as follows [28]:

$$\Delta S(E1) = -\frac{3}{2\pi}e^2\langle\Psi^0|\sum_{i<j} r_{ij}^2 v^\tau(r_{ij}) \times[t_x(i)t_x(j) + t_y(i)t_y(j)]|\Psi^0\rangle. \tag{21}$$

Here $\mathbf{t} = \frac{1}{2}\boldsymbol{\tau}$. By calculating the expectation value in Eq. (21) for the static solution $\Psi^0 = \Phi(\mathbf{Z}^0)$, we can obtain the values $S(E1)$ and κ.

In Table II, the calculated values of $S(E1)$ and κ are shown. To demonstrate that the sum rule is kept in the present framework of the time-dependent AMD, we compare the value $S(E1) = S(\mathrm{TRK}) + \Delta S(E1)$ given by the static calculations with the EWSR value $S(E1;\mathrm{total})$ that we obtained by integrating the strengths of Eq. (18) calculated with the time-dependent AMD. As shown in Table II, the sum rule $S(E1) = S(E1;\mathrm{total})$ is practically satisfied. It is reasonable because the present calculation is regarded as a method based on the small-amplitude TDHF. The enhancement factor κ is 0.71 and 0.74 for ^{12}C and ^{18}O, respectively, and it is $\kappa = 0.6$–0.7 for the neutron-rich Be, B, and C isotopes. These are consistent with $\kappa = 0.4$–0.8 because of the effect of the exchange mixtures of two-body interactions explained in Ref. [29]. In the shell-model calculations [13,17], the values $\kappa = 40\%$–50% for ^{12}C and ^{18}O are obtained for $S(E1; E_x < 40$ MeV) integrated up to 40 MeV, while $\kappa = 0.13$ for $S(E1; E_x < 40$ MeV) in ^{18}O is obtained by the quasiparticle random-phase approximation (QRPA)+phonon-coupling model [16]. In the experimental photonuclear reactions, the observed cross section integrated up to 30 MeV for ^{12}C [30] exhausts 63% of the TRK

TABLE II. The EWSR values of $E1$ transitions. The $S(E1;\text{total})$ values are obtained by integration of the strengths up to a large enough energy $E_x = 100$ MeV in the time-dependent calculations of the AMD. The enhancement $\Delta S(E1) = S(E1) - S(\text{TRK})$ is given by the ground-state expectation values of the double commutator, Eq. (21). Here we ignore the contribution of the spin-orbit force. The values of the enhancement factor $\kappa = S(E1)/S(\text{TRK}) - 1$ are also shown. The unit is MeV e^2 fm^2 for the EWSR values.

Isotope	$S(E1;\text{total})$	$S(\text{TRK})$	$\Delta S(E1)$	$S(E1)$	$S(E1;\text{total})/S(E1)$ (%)	κ
^{8}Be	51	30	21	51	100	0.71
^{10}Be	58	36	23	58	99	0.63
^{14}Be	69	42	27	69	99	0.62
^{11}B	67	40	27	67	99	0.66
^{15}B	81	49	32	81	100	0.63
^{17}B	85	52	33	86	100	0.63
^{12}C	76	44	32	76	100	0.71
^{16}C	92	56	36	92	100	0.65
^{18}C	98	59	39	98	100	0.65
^{20}C	103	62	40	102	101	0.66
^{18}O	115	66	49	115	100	0.74

sum-rule value, and 90% of $S(\text{TRK})$ is exhausted by the EWSR integrated up to 42 MeV in ^{18}O [31]. As shown later, the EWSR is dominated by the GDR in the present results. It means that the calculated GDR should be quenched and the large fraction of the strength should be in the higher-energy region than the GDR.

C. Dipole resonances

1. ^{12}C *and* ^{18}O

We first show the results of the dipole resonances in ^{12}C and ^{18}O and compare the results with other theoretical calculations and experimental data to see the validity of the present method. The photonuclear cross sections of ^{12}C and ^{18}O are plotted as functions of the excitation energy in Figs. 3 and 4, respectively. Thin dash-dotted, solid, and dotted curves indicate the contribution of vibration for the x, y, and z directions, respectively. Here and hereafter, we chose the x, y, and z axis as $\langle\Psi^0|x^2|\Psi^0\rangle \leqslant \langle\Psi^0|y^2|\Psi^0\rangle \leqslant \langle\Psi^0|z^2|\Psi^0\rangle$ and $\langle xy\rangle = \langle yz\rangle = \langle zx\rangle = 0$. The thick solid curves correspond to the total strengths. We use the smoothing parameter $\Gamma = 1, 2, 4$ MeV. In the present results, the GDR peak lies at $E_x = 26$ MeV and $E_x = 28$ MeV in ^{12}C and ^{18}O, respectively. These peak positions are about 4 MeV higher than the observed GDR peaks [30–33] and also higher than other theoretical values of the shell model [13,17] and the QRPA calculations [16]. Compared with the observed photonuclear cross section, here a smoothing parameter $\Gamma > 4$ MeV is needed to reproduce the width of the GDR. The reason for such a large Γ is considered to be due to the limitation of the present model space and lack of the effects of continuum states. For a quantitative discussion of the magnitude of the GDR strength, further quenching and spreading are needed in the present calculations.

Although the quantitative description of the peak positions and the magnitudes of the GDR are not sufficient, the characteristic behavior of the calculated cross section is in reasonable agreement with that of the experimental data and is consistent with other theoretical calculations. Because the ground state of ^{12}C is a oblate state, the vibration for each of the y and z axes forms a peak in the same energy, which results in an enhancement of the lower part of the GDR. In the results of ^{18}O, significant dipole strengths are distributed in the energy region below the GDR because of the valence neutrons. The strong resonances have been experimentally observed in the region 10−15 MeV [20,31], and about 8% [20] of the TRK sum rule is exhausted by the integrated strength of the experimental data up to $E_x = 15$ MeV. These low-lying resonances are well described by the shell-model calculations [13], which give $S(E1; E_x < 15\,\text{MeV})/S(\text{TRK}) = 6\%$. In the present results, the excitation energies of these low-lying resonances seem to be overestimated compared with those of the shell-model and QRPA calculations as well as the GDR. Namely, the strengths of the low-lying peaks are distributed in the $E_x = 15$–20 region, and $S(E1; E_x < 17\ \text{MeV})/S(\text{TRK}) = 6\%$ and $S(E1; E_x < 15\ \text{MeV})/S(\text{TRK}) = 3\%$ in the present results. Considering the shift of the excitation energies, we can state that the calculated strengths of the low-lying resonances reasonably agree with the experimental data.

One of the reasons for the overestimating excitation energies of the dipole resonances is because the surface diffuseness may be underestimated by the simple AMD wave function. It might be improved by the extension of the model wave function such as deformed-base AMD proposed Kimura *et al*. [34].

2. C, B, and Be isotopes

Next we investigate the dipole resonances in neutron-rich Be, B, and C isotopes. We show the $E1$ strengths in ^{8}Be, ^{10}Be, and ^{14}Be in Fig. 5, and the photonuclear cross sections in the left-hand column of Fig. 6.

In ^{10}Be, the dipole resonances in ^{10}Be can be decomposed into two parts, $E_x < 15$ MeV and $E_x > 20$ MeV. The former consists of the soft resonances with the dominant strengths in $10 < E_x < 15$ MeV. The latter contains the GDR with the double-peak structure with 7–8-MeV energy splitting, which is similar to that of ^{8}Be. In the $E_x < 5$ MeV region, we find

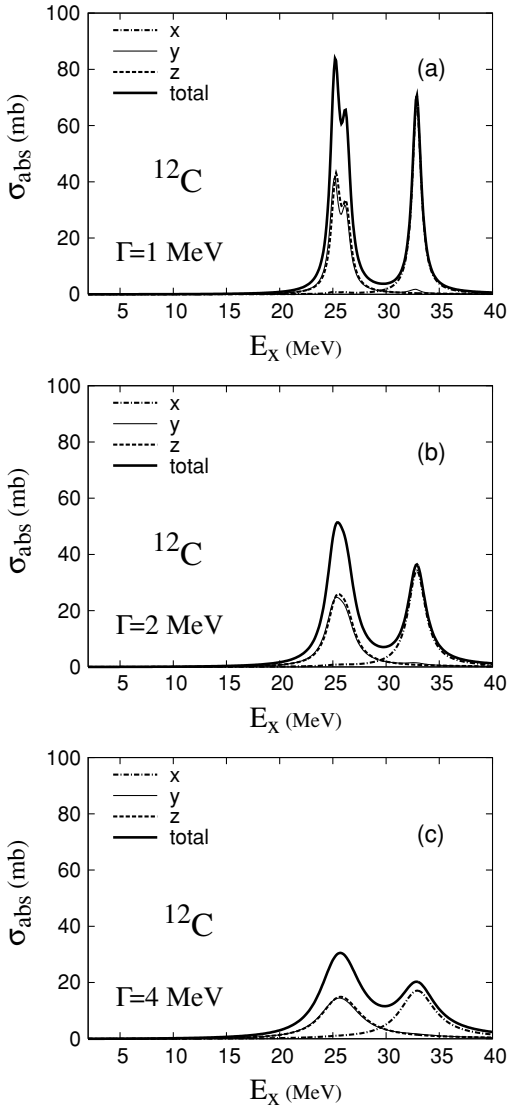

FIG. 3. The calculated photonuclear cross section of ^{12}C. The smoothing parameters $\Gamma = 1$, 2, 4 MeV are used. Thin dash-dotted, solid, and dotted curves are the contributions of vibration for the x, y, and z directions, respectively. The thick solid curves indicate the total strengths.

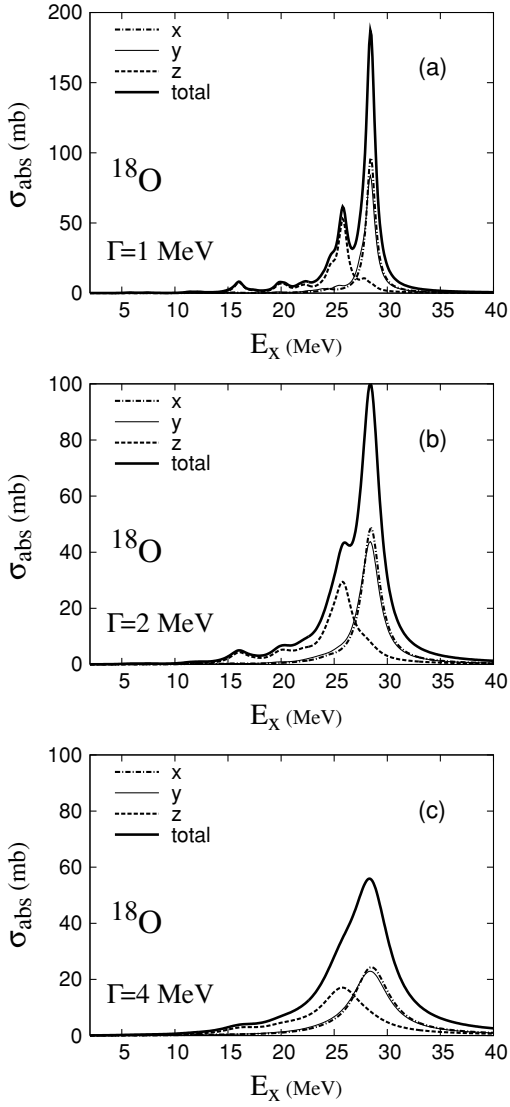

FIG. 4. The calculated photonuclear cross section of ^{18}O. The smoothing parameters $\Gamma = 1$, 2, 4 MeV are used. Thin dash-dotted, solid, and dotted curves are the contributions of vibration for the x, y, and z directions, respectively. The thick solid curves indicate the total strengths.

a peak with the strength $B(E1) = 0.06\ e^2\ \mathrm{fm}^2$. We consider that this is a 1^- state and corresponds to the known 1^- state at 5.96 MeV. The present low-lying peaks in the $10 < E_x < 15$ MeV region originate in the cluster structure. The details are discussed in the next section. In the TDHF + absorbing boundary-condition (ABC) calculations, the strengths of the soft $E1$ resonances [18] are not significant in ^{10}Be. On the other hand, the GDR of the TDHF + ABC calculations in ^{10}Be is consistent with the present results.

In ^{14}Be, the GDR splits into two peaks at $E_x = 15$ MeV and at $E_x > 25$ MeV. The lower peak appears in the vibration along the longitudinal axis (z). As seen in Figs. 1 and 2, ^{14}Be has a large prolate deformation of the neutron density as well as the large neutron radius, and hence it has the enhanced neutron skin structure along the longitudinal direction. The decrease of the excitation energy of the lower GDR peak is naturally understood because of the developed neutron skin. Also in the TDHF + ABC calculations [18], the GDR in ^{14}Be for the longitudinal motion appears at $E_x = 15$ MeV, while the higher peak for the transverse motion is around $E_x = 25$ MeV. Although the peak position of the GDR for each direction is similar to the present results, the GDR is not splitting in the TDHF + ABC results because the widths are largely spread. Another difference with the present results is that there exists a very soft resonance at $E_x \sim 5$ MeV in TDHF + ABC. These differences seem natural for the following reason: The spreading and quenching of the GDR may be large in ^{14}Be, which has a small neutron separation energy, and therefore the dipole strengths should be affected by the continuum states and the long tail of the neutron halo structure. These effects are not taken into account in the present framework,

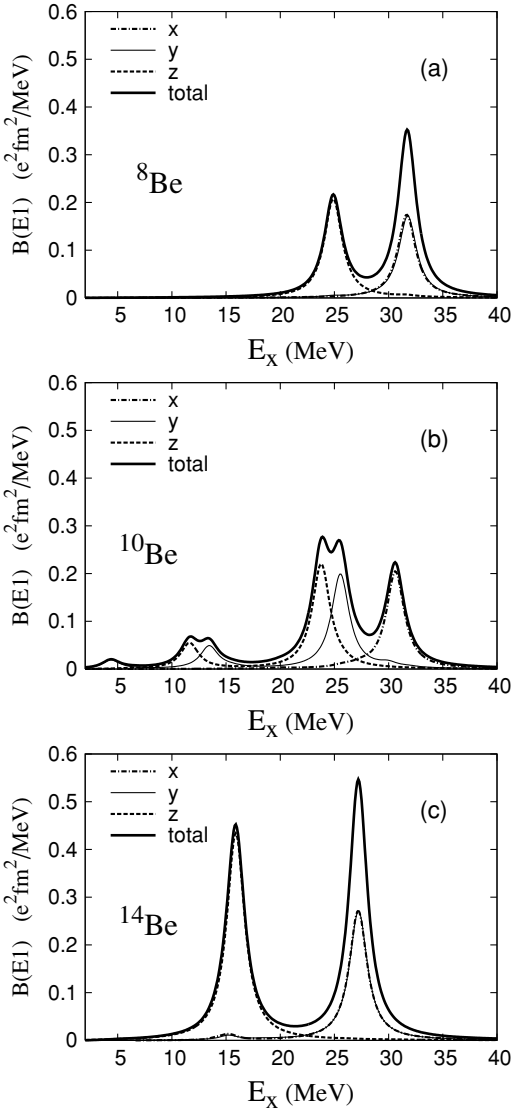

FIG. 5. The calculated $E1$ transition strengths of ^{8}Be, ^{10}Be, and ^{14}Be. The smoothing parameter is chosen to be $\Gamma = 2$ MeV. Thin dash-dotted, solid, and dotted curves are the contributions of vibration for the x, y, and z directions, respectively. The total strengths are shown by the thick solid curves.

but they are included in the TDHF + ABC. In the shell-model calculations, the large $E1$ strength is found in the low-energy region ($5 < E_x < 15$ MeV) when the *fp* shell configurations are included with the WBP interaction [15].

The $E1$ strengths and the photonuclear cross sections in B isotopes are shown in Figs. 7 and 6. In the B isotopes, the feature of the GDR changes, reflecting the variation of the deformation as the neutron number increases. In ^{15}B, two peaks of the GDR appear at $E_x = 20$ and 27 MeV [see Fig. 7(b)]. Because of the prolate deformation, the lower GDR at $E_x =$ 20 for the longitudinal (z-direction) vibration has a smaller strength than that of the higher one. The excitation energy of the GDR is smaller than that of ^{11}B. One of the unique features in ^{15}B is that a soft resonance appears in the $E_x = 10$–17 MeV region, which exhausts 16% of the S(TRK) value. This soft resonance arises from the longitudinal vibration and decouples energetically from the GDR region ($E_x > 17$ MeV). In ^{17}B, the GDR peaks spread over a wide energy region because of the triaxial deformation. The peak position of the lowest GDR further shifts toward the low-energy region: $E_x \sim 18$ MeV. We cannot find a strong soft $E1$ resonance other than the GDR in ^{17}B.

We show the results of C isotopes in Figs. 8 and 6. In a comparison between B (Fig. 7) and C isotopes (Fig. 8), it is found that the feature of the dipole transitions in ^{16}C is quite similar to that in ^{15}B, which has the same neutron number ($N =$ 10) with ^{16}C. Namely, the dipole strength for the longitudinal (z-axis) vibration splits into two peaks, the GDR at $E_x =$ 22 MeV and a soft resonance at $E_x = 14$ MeV. As a result, ^{16}C has a significant dipole strength in the low-energy region ($E_x < 17$ MeV) below the GDR region. This soft dipole resonance at $E_x = 14$ MeV is consistent with the shell-model calculations [17], in which a remarkable peak is found at the same energy. In ^{18}C, because it has a triaxial deformation, as does ^{17}B, the shape of the strength function in the GDR region is similar to that of ^{17}B, though the peak positions are slightly higher than those of ^{17}B. A difference between ^{18}C and ^{17}B is the soft dipole strengths in the energy region $E_x < 17$ MeV. Although there is no noticeable peak in this energy region, we find some fractions of the dipole strengths in ^{18}C rather than in ^{17}B. In ^{20}C with an oblate deformation, the shape of the strength function $dB(E1, \omega)/d\omega$ is similar to the ^{12}C, whereas the peak positions are 4–5 MeV lower than those of ^{12}C.

V. DISCUSSION

As shown before, the remarkable peaks of the soft resonances are found in the dipole strengths of ^{10}Be, ^{15}B, and ^{16}C. They are clearly separated from the GDR region. It is natural to expect that these soft resonances arise from the coherent excitations of excess neutrons. To link the $E1$ resonances with collective motions, we analyze the time evolution of the single-particle wave functions. In the time-dependent AMD, the expectation value of the dipole operator $\mathcal{M}(E1, \mu = 0)$ for $\Psi(t) = \Phi[\mathbf{Z}(\mathbf{t})]$ is directly related to the real part of the centers of the single-particle Gaussian wave packets:

$$\langle \Psi(t)|\mathcal{M}(E1, \mu = 0)|\Psi(t)\rangle = \frac{Ne}{A}\sum_{i=1}^{Z}\mathrm{Re}\left[\frac{Z_{iz}(t)}{\sqrt{\nu}}\right] - \frac{Ze}{A}\sum_{i=Z+1}^{A}\mathrm{Re}\left[\frac{Z_{iz}(t)}{\sqrt{\nu}}\right], \quad (22)$$

where the ith particle is a proton (neutron) for $i = 1, \ldots, Z(Z+1, \ldots, A)$, and Z_{iz} is the z component of the center $\mathbf{Z}_i$ for the ith single-particle Gaussian wave function. It should be stressed that the $E1$ excitations are expressed by the motion of the centers of single-particle Gaussian wave packets. Because the $E1$ strength is given by the Fourier transform of Eq. (22) as explained in Sec. II, we can examine separately the contribution of each single-particle wave-packet motion to the dipole strengths by Fourier transform of $\mathrm{Re}[Z_{iz}(t)/\sqrt{\nu}]$, and see explicitly the collective modes. As discussed later, in the case in which a collective mode appears because of the

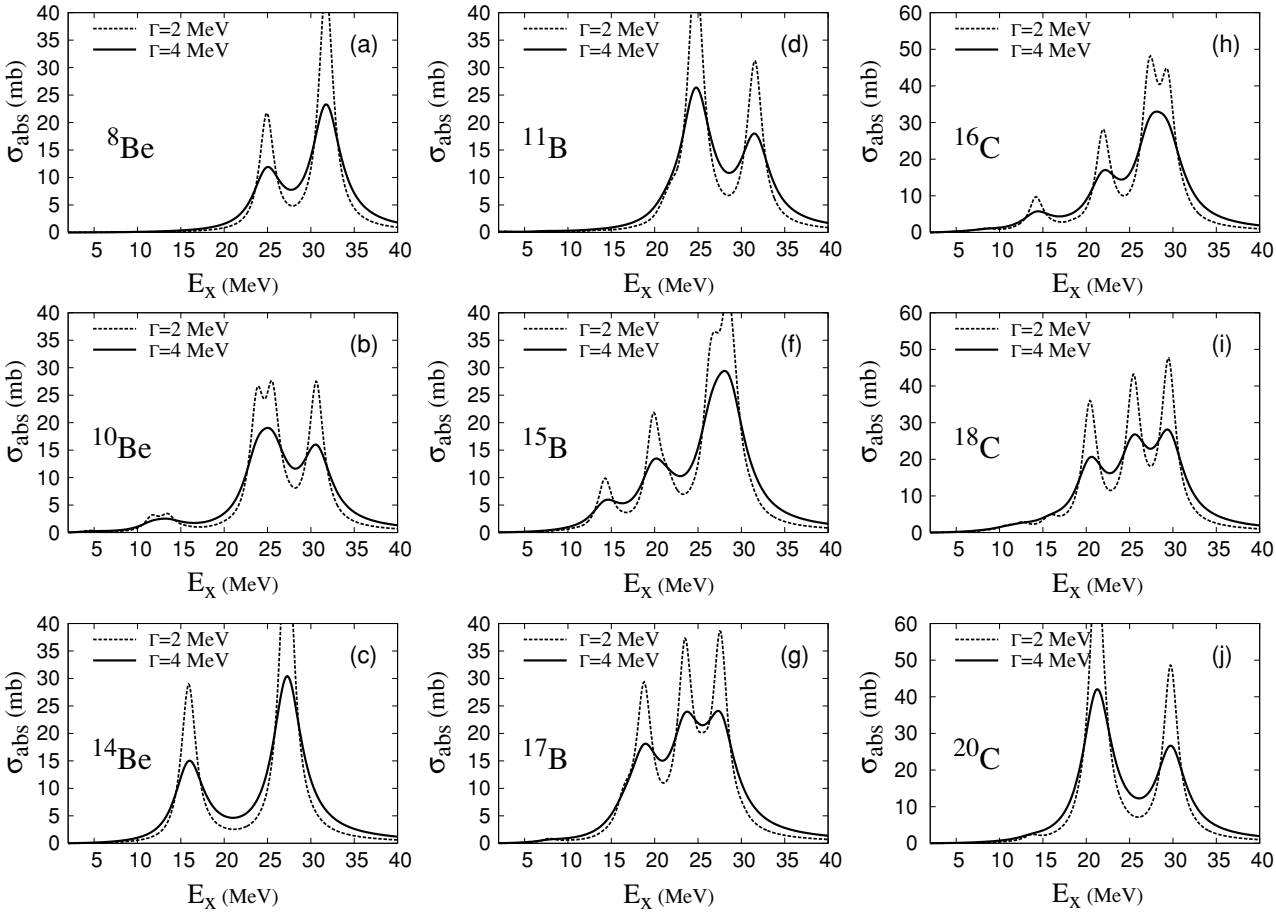

FIG. 6. The calculated photonuclear cross section in (a)^{8}Be, (b)^{10}Be, (c)^{14}Be, (e)^{11}B, (f)^{15}B, (g)^{17}B, (h)^{16}C, (i)^{18}C, (j)^{20}C. The smoothing parameters are chosen to be $\Gamma = 2$ MeV (dashed curves) and 4 MeV (solid curves).

intercluster motion, the mode can be seen as the peak at the corresponding excitation energy in the sum of the components for nucleons in each cluster:

$$-\frac{1}{\pi\epsilon}\mathrm{Im}\int dt \sum_{i\in C_k}\mathrm{Re}[Z_{iz}/\sqrt{\nu}]e^{i\omega t}, \tag{23}$$

where $C_1, C_2, \ldots,$ are the constituent clusters and ϵ is the same parameter as in Eq. (12).

In Fig. 9, we illustrate the density distributions and the spatial configuration of the Gaussian centers $\mathrm{Re}[\mathbf{Z}_i/\sqrt{\nu}]$ in the static solution of ^{16}C. There is a difference between proton and neutron densities in the ground state. The $E1$ transitions are described by the small-amplitude motion around this static solution. We see a $2n + {}^{12}\mathrm{C} + 2n$ configuration in the spatial configuration of the Gaussian centers, which forms the prolate neutron deformation with the longitudinal z axis. After the instantaneous external dipole field $\mathcal{M}(E1, \mu = 0)$ is imposed, four valence neutrons move coherently against the core ^{12}C with the oscillation energy $E_x \sim 14$ MeV to cause the soft dipole peak. On the other hand, it is found that the strengths in the GDR region ($E_x > 20$ MeV) arise from the motion of the nucleons within the ^{12}C core. In Fig. 10(a), we show the amplitudes of the motion for four valence neutrons, six protons, and six neutrons in the ^{12}C core. It is found that the valence neutrons move with negative amplitudes against six protons and six neutrons in the $E_x \sim 14$ MeV region, whereas the dipole strengths in the GDR region are dominated by the relative motion between six protons and six neutrons inside the ^{12}C core. The reason why four neutrons move coherently in the $2n + {}^{12}\mathrm{C} + 2n$ configuration is easily understood as follows. Because the $2n + {}^{12}\mathrm{C} + 2n$ configuration is linear, one can consider a configuration with two dineutrons on the opposite sides of the core (^{12}C). Let us imagine the inert three clusters ($2n + {}^{12}\mathrm{C} + 2n$), which are connected with two identical springs, as shown in Fig. 9(d). In the motion along the longitudinal axis, there are two eigenmodes of the oscillation. One is the mode in which two dineutrons move in phase and the core moves in the opposite way, and the other is the one with the opposite motion of the dineutrons to each other. The former corresponds to the isovector-dipole mode. Thus the coherent motion of the valence neutron can be interpreted by the relative motion in the $2n + {}^{12}\mathrm{C} + 2n$ configuration. The soft dipole resonance that is due to the excess neutrons in the present result of ^{16}C corresponds well to the shell-model calculations [13], in which the $0p \to 1s0d$ and $1s0d \to 0f1p$ transitions work coherently to enhance the strength at $E_x = 12$–14 MeV in ^{16}C.

We show the density distribution of the ground state of ^{10}Be in Fig. 11. To understand collective motion for the

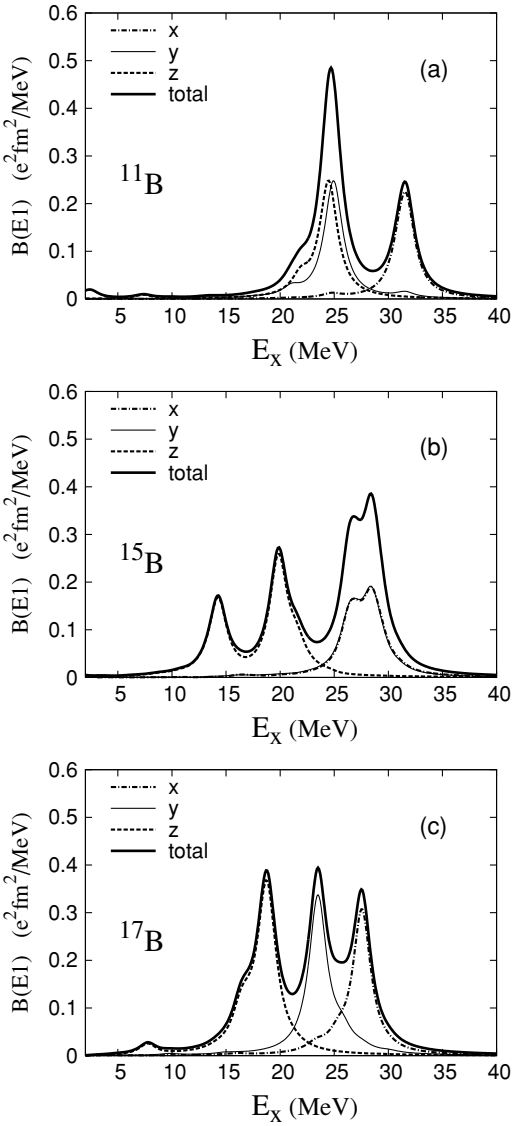

FIG. 7. The calculated $E1$ transition strengths of ^{11}B, ^{15}B, and ^{17}B. The smoothing parameter is chosen to be $\Gamma = 2$ MeV. Thin dash-dotted, solid, and dotted curves are the contributions of vibration for the x, y, and z directions, respectively. The total strengths are shown by the thick solid curves.

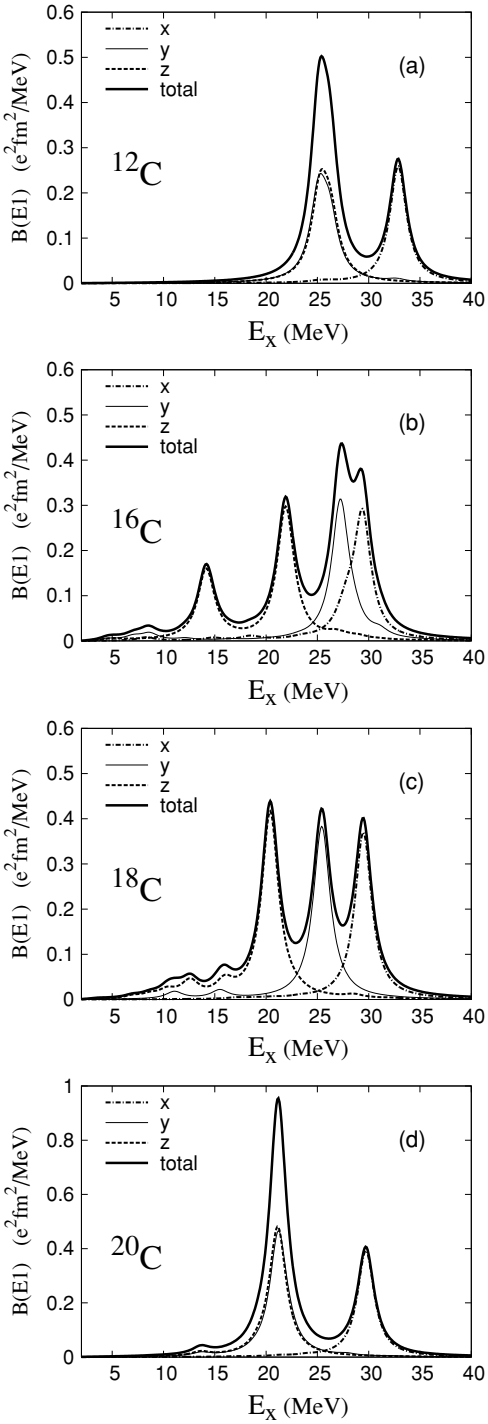

FIG. 8. The calculated $E1$ transition strengths of ^{12}C, ^{16}C, ^{18}C, and ^{20}C. The smoothing parameter is chosen to be $\Gamma = 2$ MeV. Thin dash-dotted, solid, and dotted curves are the contributions of vibration for the x, y, and z directions, respectively. The total strengths are shown by the thick solid curves.

soft dipole resonances, it is useful to regard the ^{10}Be as the $\alpha + {}^6$He cluster state. In the analysis of motion of Gaussian centers, it is found that the strengths at $E_x = 10$–15 MeV contain two independent modes. One is the intercluster motion between α and ^{6}He, which contributes to the resonance at $E_x = 12$ MeV in the longitudinal vibration along the z axis. The other is the coherent motion of the valence neutron against the core ^{8}Be, which results in the resonance at $E_x = 14$ MeV in the vibration along the y axis. In Fig. 10(c), we show the amplitudes of the $\alpha - {}^6$He intercluster motion. It has a dominant peak at $E_x = 10$–15 MeV, which corresponds to the soft peak in the z component. On the other hand, as seen in Fig. 10(b), where we show each of the amplitudes of $4n$, $4p$ and the two valence neutrons, the relative motion between four protons and four neutrons contributes to the GDR peak. In other words, the GDR is described by the motion inside the core ^{8}Be. Also in ^{15}B, we find that the coherent motion of the valence neutrons contributes to an enhancement of the strengths of the soft resonance. It is concluded that the remarkable peaks at $E_x = 10-15$ MeV in ^{16}C, ^{10}Be, and ^{15}B arise from the

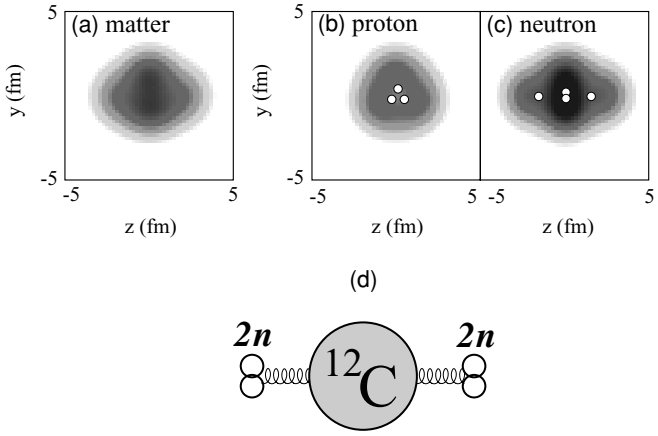

FIG. 9. The density distribution of the ground state of ^{16}C. The densities are integrated along the x axis: (a) matter density, (b) proton density, (c) neutron density. The spatial configuration of the centers of single-particle Gaussian wave packets for protons and neutrons are also plotted by open circles in (b) and (c), respectively. Each circle consists of a spin-up nucleon and a spin-down nucleon. (d) The schematic figure for the configurations of the Gaussian centers in ^{16}C written by $2n + {}^{12}\mathrm{C} + 2n$.

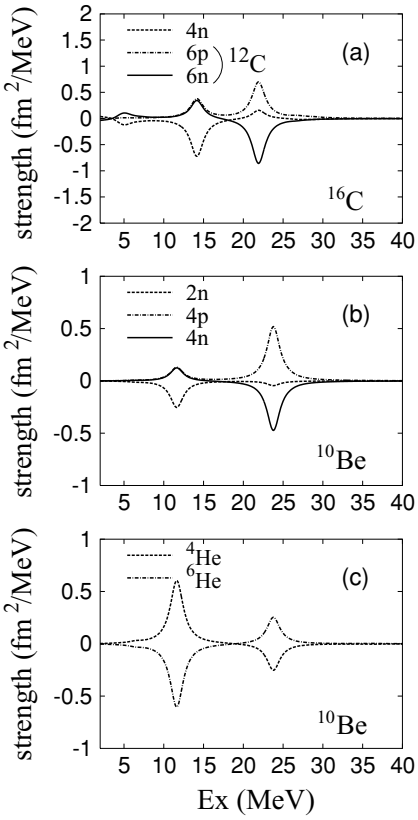

FIG. 10. Amplitudes of the motion of the Gaussian centers in the responses of ^{16}C and ^{10}Be with an instantaneous dipole field along the z axis. The amplitudes are given by the Fourier transform of positions of the Gaussian centers, as shown by expression (23). We divide A nucleons into groups, $C_1, C_2, \ldots$, and sum up the components for the nucleons in each group. (a) Motion of the Gaussian centers in ^{16}C. C_1 consists of four valence neutrons, and C_2 (C_3) contains six protons (neutrons) in the ^{12}C core. (b) Motion in ^{10}Be. C_1, C_2, and C_3 consist of two valence neutrons, four protons, and four residual neutrons. (c) Relative motion between ^{4}He (C_1) and ^{6}He (C_2) clusters in ^{10}Be. The dotted, dash-dotted, and solid curves correspond to C_1, C_2, and C_3, respectively.

coherent motion of the valence nucleons, which decouples from the motion inside the core.

We show the calculated photonuclear cross section in Fig. 6 in Subsec. 4.C.2. The shape of the strength function in the GDR region ($E_x > 17$ MeV) has a close relation with the deformation of the system. In oblate systems such as ^{11}B and ^{20}C as well as ^{12}C, the GDR splits into two parts. The lower GDR peak has large transition strengths. In the neutron-rich nucleus, ^{20}C, the peak position of the GDR is the lowest among the three nuclei. Also in the ^{8}Be and ^{14}Be with the prolate deformation, the GDR splits into two, but the higher GDR has a larger strength in contrast to the oblate deformation. The lower resonance in ^{14}Be appears at $E_x = 15$ MeV. In triaxial nuclei such as ^{17}B and ^{18}C, the GDR consists of three peaks with 5 MeV of the energy splitting. However, considering the spreading of the widths, three peaks may overlap to form a broad structure in the $E_x = 15$–30 MeV. ^{10}Be and ^{16}C have ground states with opposite deformations between proton and neutron densities. In spite of these unusual properties of the deformations, we cannot find an abnormal feature of the dipole strength in the GDR region in these nuclei. As explained before, the remarkable soft peaks appear at $E_x = 10$–15 MeV because of the motion of the valence nucleons against the core, whereas the GDR at $E_x > 17$ MeV arises from the vibration within the core. Therefore it is considered that the GDR may reflect mainly the features of the core nuclei instead of the deformations of the total system. In fact, the GDR of ^{10}Be lies at an excitation energy similar to that of ^{8}Be.

Below the GDR region, we find the significant strengths of the soft resonances in such neutron-rich nuclei as ^{10}Be, ^{15}B, ^{16}C, and ^{18}C that are due to the excess neutrons. In particular, ^{10}Be, ^{15}B, and ^{16}C have remarkable soft peaks, which are decoupled from the GDR. In the neutron-rich nuclei, the cluster sum rule [35] is a convenient measure for estimating the contribution of the motion of the excess neutrons in the dipole strengths [36]. Assuming clustering with a core and N_v valence neutrons, we consider the core cluster with $Z_1 = Z$, $N_1 = N - N_v$, and the valence cluster with $Z_2 = 0$, $N_2 = N_v$. The cluster sum rule is given as

$$S_{\mathrm{clust}} = \frac{\hbar^2}{2m}\frac{9}{4\pi}\frac{(Z_1N_2 - Z_2N_1)^2}{A(Z_1+N_1)(Z_2+N_2)}e^2 = \frac{\hbar^2}{2m}\frac{9}{4\pi}\frac{Z^2N_v^2}{A(A-N_v)N_v}e^2. \quad (24)$$

This value is the remainder when one subtracts the core contribution of the classical EWSR from the total S(TRK) value. Consequently S_{clust} is the margin that indicates the contribution of the excess neutrons. The integrated strength of the low-energy resonances should be compared with S_{clust} to see the softness and collectivity of the resonances that are

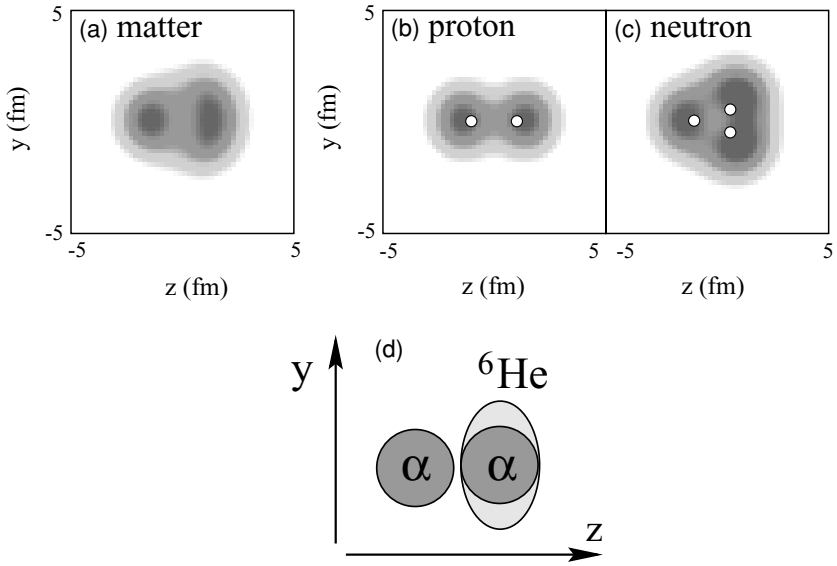

FIG. 11. The density distribution of the ground state of ^{10}Be. The densities are integrated along the x axis: (a) matter density, (b) proton density, (c) neutron density. The spatial configurations of the centers of single-particle Gaussian wave packets for protons and neutrons are also plotted by open circles in (b) and (c), respectively. Each circle consists of a spin-up nucleon and a spin-down nucleon. (d) The schematic figure for the structure of ^{10}Be with an $\alpha + {}^6$He configuration.

due to the valence neutron motion against the core. In Table III, the calculated EWSR for the low-lying resonances are listed with the values of the classical TRK sum rule and the cluster sum rule ($S_{\rm clust}$). In the derivation of the cluster sum rule $S_{\rm clust}$, the core cluster is assumed to be ^{8}Be, ^{11}B, ^{12}C, and ^{16}O, in Be, B, C, and O isotopes, respectively. We show the EWSR values integrated up to $E_x < 15$ MeV and $E_x < 17$ MeV in the present results and the EWSR with other calculations. The ratios of the EWSR to S(TRK) and $S_{\rm clust}$ are shown in Figs. 12(a) and 12(b), respectively. In C isotopes, $S(E1; E_x <$ 17 MeV) is the largest in ^{16}C and it declines in further neutron-rich C isotopes. The present results of C isotopes well agree with the shell-model calculations [13]. A similar feature is also found in B isotopes. Namely, $S(E1; E_x < 17$ MeV) is the largest in ^{15}B and it decreases in further neutron-rich nucleus ^{17}B. The striking point is that the EWSR for the low-lying resonances is remarkably enhanced in the moderately neutron-rich nuclei with an appropriate number of excess neutrons, but it is suppressed in very neutron-rich nuclei. It is reasonable because the enhancement of the soft dipole strengths is due to the coherent motion of the valence neutrons relative to the core. It means that the decoupled collective modes appear based on the relative motion between the core and the valence neutrons and the motion inside the core in moderately neutron-rich nuclei such as ^{15}B and ^{16}C. On the

TABLE III. The EWSR for the soft dipole resonances. The energy-weighted sums integrated up to $E_x < 17$ MeV and $E_x <$ 15 MeV are shown in the fourth and fifth columns, respectively. The core clusters in the derivations of the cluster sum rule $S_{\rm clust}$ are ^{8}Be, ^{11}B, ^{12}C, and ^{16}O in Be, B, C, and O isotopes, respectively. The smoothing parameter is chosen to be $\Gamma = 2.0$ MeV. The unit is e^2 fm^2 MeV.

Isotope	S(TRK)	$S_{\rm clust}$	$S(E1)$	
			$E_x < 17$ MeV	$E_x < 15$ MeV
^{8}Be	29.7	–	0.3	0.2
^{10}Be	35.6	5.9	4.3	4.0
^{14}Be	42.4	12.7	19.0	3.1
^{12}C	44.5	–	0.5	0.3
^{16}C	55.6	11.1	8.3	6.9
^{18}C	59.3	14.8	5.6	3.4
^{20}C	62.3	17.8	2.3	1.6
^{11}B	40.5	–	1.1	0.8
^{15}B	49.4	9.0	8.2	6.4
^{17}B	52.3	11.9	5.8	1.7
^{18}O	65.9	6.6	4.0	1.5

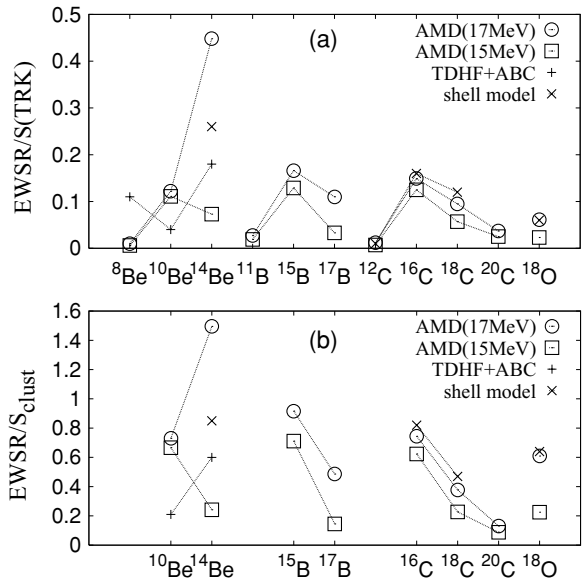

FIG. 12. The ratio of the EWSR integrated for the soft dipole resonances to S(TRK) and $S_{\rm clust}$. Circles indicate the ratio for $S(E1; E_x < 17$ MeV) and squares are for $S(E1; E_x < 15$ MeV). The smoothing parameter is chosen to be $\Gamma = 2.0$ MeV. The results of TDHF + ABC for $S(E1; E_x < 15$ MeV) in Be isotopes are indicated by "+." The symbols × indicate the results of the shell-model calculations for $S(E1; 5 < E_x < 15$ MeV), $S(E1; E_x < 14$ MeV), and $S(E1; E_x < 15$ MeV) in Be [15], C [17], and O [13], respectively.

other hand, in further neutron-rich nuclei $N > 10$, the neutron skin developes, and hence the motion of the excess neutrons is not decoupled but join the neutrons inside the core. As a result, in ^{17}B and ^{20}C, the soft dipole mode is assimilated into the GDR, and the excitation energy of the GDR decreases. Also in ^{10}Be, the EWSR for the low-lying resonances is significant as well as in ^{15}B and ^{16}C. In these nuclei, the cluster sum-rule value $S_{\rm clust}$ is almost exhausted by the calculated $S(E1; E_x < 17$ MeV). In ^{14}Be, the $S(E1; E_x < 17$ MeV) is very large because of the peak at $E_x = 16$ MeV. The reason for the enhanced $S(E1; E_x < 17$ MeV) in ^{14}Be is different from that for other nuclei (^{10}Be,^{15}B and ^{16}C). In the case of ^{14}Be, the enhanced $S(E1; E_x < 17$ MeV) does not originate in the soft resonance decoupled from the GDR, but the GDR for the longitudinal vibration itself contributes to the EWSR for the low-energy region because it becomes soft because of the prolate deformation with a developed neutron skin structure.

VI. SUMMARY

We applied a method of the time-dependent AMD to studies of dipole transitions in light neutron-rich nuclei. We investigated the $E1$ resonances in Be, B, and C isotopes. It was found that remarkable peaks appear in ^{10}Be, ^{15}B, and ^{16}C at $E_x = 10$–15 MeV, which almost exhaust the values of the cluster sum rule. These soft dipole resonances arise from the relative motion between excess neutrons and the core, which is decoupled from the motion inside the core. In other words, these soft resonances appear because of the excitation of the excess neutrons around the rather hard core. This nature of the neutron excitation and the inert core may have a link with such ground-band properties of ^{16}C as the unusually small $B(E2; 2^+_1 \to 0^+_1)$ [37], which has been recently investigated in theoretical and experimental studies [3,38–40]. In further neutron-rich B and C isotopes with $N > 10$, the strength for the soft dipole resonances declines compared with that of ^{15}B and ^{16}C. It is considered to be because the motion of the excess neutrons is assimilated into the neutron motion within the core. As a result, the excitation energies of the GDR decrease with the enhancement of the neutron skin. It is striking that the strength for the soft dipole resonances does not necessarily increase with the increase of the excess neutrons. Instead, the feature of the soft resonances rapidly changes depending on the proton and neutron numbers of the system. The key of the soft dipole resonance with a remarkable strength is how the coherent motion of the valence neutrons is decoupled from the motion inside the core.

The present method based on the time-dependent AMD is regarded as types of small-amplitude TDHF calculations within the AMD model space. The point of the method is that we are able to study dipole resonances within a framework that can describe cluster aspect. In the AMD approach, the dipole excitations are expressed by the motion of single-particle Gaussian wave packets, because the expectation value of the dipole operator is directly related to the centers of the Gaussian wave packets. One of the advantages of time-dependent AMD is that we can link the excitations with such collective modes as core vibration, core-neutron motion, and intercluster motion, which should be important for understanding the role of the excess neutrons in the dipole resonances.

Recently, extended methods of time-dependent mean-field calculations have been proposed and applied to the dipole transitions in neutron-rich nuclei. In the TDHF + ABC approach, which has been applied to deformed neutron-rich nuclei by Nakatsukasa and Yabana [18], the effects of continuum states are taken into account. Another method is the time-dependent density-matrix theory that has been applied to ^{22}O by the incorporation of two-body correlations [7]. In this paper, the contributions of continuum states are omitted, and detailed descriptions of wave functions and two-body correlations should be insufficient, as the model space is a simple AMD wave function written by a Slater determinant of Gaussian wave packets. Therefore we use an artificial smoothing parameter to simulate the width of the dipole resonances, because it is difficult to describe the escape and the spreading widths of the resonances in the present framework. Further extensions of the model are essential for providing quantitative discussions of the excitation energies and the strengths of the dipole resonances in nuclei near the drip line. It should be necessary to solve the remaining problem of the soft resonances in halo nuclei [4–6,12,14,19,21].

We comment that the usual AMD wave functions applied to the nuclear structure study are the advanced ones with some extensions, such as parity and spin projections, deformed Gaussian base, and a generator coordinate method [22,34,41–43], though the present AMD wave function is the simplest one, with no extension. A combination of the time-dependent method and the extended AMD wave functions is needed to include higher correlations beyond the present calculations and also to obtain a better description of the ground-state properties. We think that a possible modification to the parity and spin projections is a time-dependent AMD method within a model space of the linear combination of Slater determinants, which is beyond mean-field approaches. Such a method of linear combination may be effective for taking into account the contributions of higher excitations than $1p$–$1h$. It could make the artificial smoothing parameter Γ smaller than the present value, because the effects of spreading widths might be incorporated. Other possible modifications by the parity and spin projections are related to the collective deformations. For example, parity asymmetric features of the static solutions might enhance the parity-projected calculations. It is also expected that soft $E1$ modes could develop because of octupole vibration in a deformed system. Studies of $E1$ response in $N = 8$ systems remain to be done because we could not calculate it because of the difficulties in obtaining stable solutions with the present method of the simple AMD. Moreover, the interaction dependence of the dipole transitions is also another remaining problem.

ACKNOWLEDGMENTS

The authors thank H. Horiuchi for many discussions. Y. K. is also grateful to T. Nakatsukasa and M. Tohyama for valuable comments. Discussions during the workshop YITP-W-05-01 on "New Developments in Nuclear Self-Consistent Mean-Field Theories," which was held at the Yukawa Institute for

Theoretical Physics at Kyoto University, were useful in helping use complete this work. The computational calculations in this work were supported by the Supercomputer Projects of High Energy Accelerator Research Organization. This work was supported by the Japan Society for the Promotion of Science and a Grant-in-Aid for Scientific Research of the Japan Ministry of Education, Science and Culture. A part of the work was performed in the "Research Project for Study of Unstable Nuclei from Nuclear Cluster Aspects" sponsored by the Institute of Physical and Chemical Research.

[1] Y. Kanada-En'yo, H. Horiuchi, and A. Ono, Phys. Rev. C **52**, 628 (1995); Y. Kanada-En'yo and H. Horiuchi, *ibid*. **52**, 647 (1995).
[2] Y. Kanada-En'yo and H. Horiuchi, Phys. Rev. C **55**, 2860 (1997).
[3] Y. Kanada-En'yo, Phys. Rev. C **71**, 014310 (2005).
[4] M. Honma and H. Sagawa, Prog. Theor. Phys. **84**, 494 (1990).
[5] T. Hoshino, H. Sagawa, and A. Arima, Nucl. Phys. **A523**, 228 (1991).
[6] H. Sagawa, N. Takigawa, and Nguyen van Giai, Nucl. Phys. **A543**, 575 (1992).
[7] M. Tohyama, Phys. Lett. **B323**, 257 (1994).
[8] I. Hamamoto, H. Sagawa, and X. Z. Zhang, Phys. Rev. C **53**, 765 (1996).
[9] I. Hamamoto and H. Sagawa, Phys. Rev. C **53**, R1492 (1996).
[10] F. Catara, E. G. Lanza, M. A. Nagarajan, and A. Vitturi, Nucl. Phys. **A624**, 449 (1997).
[11] I. Hamamoto, H. Sagawa, and X. Z. Zhang, Phys. Rev. C **57**, R1064 (1998).
[12] T. Myo, A. Ohnishi, and K. Kato, Prog. Theor. Phys. **99**, 801 (1998).
[13] H. Sagawa and T. Suzuki, Phys. Rev. C **59**, 3116 (1999).
[14] T. Suzuki, H. Sagawa, and P. F. Bortignon, Nucl. Phys. **A662**, 282 (2000).
[15] H. Sagawa, T. Suzuki, H. Iwasaki, and M. Ishihara, Phys. Rev. C **63**, 034310 (2001).
[16] G. Colo and P. F. Bortignon, Nucl. Phys. **A969**, 427 (2001).
[17] T. Suzuki, H. Sagawa, and K. Hagino, Phys. Rev. C **68**, 014317 (2003).
[18] T. Nakatsukasa and K. Yabana, Phys. Rev. C **71**, 024301 (2005).
[19] T. Nakamura *et al*., Phys. Lett. **B394**, 11 (1997).
[20] A. Leistenschneider *et al*., Phys. Rev. Lett. **86**, 5442 (2001).
[21] R. Palit *et al*., Phys. Rev. C **68**, 034318 (2003).
[22] Y. Kanada-En'yo and H. Horiuchi, Prog. Theor. Phys. Suppl. **142**, 205 (2001).
[23] A. Ono, H. Horiuchi, T. Maruyama, and A. Ohnishi, Phys. Rev. Lett. **68**, 2898 (1992).
[24] A. Ono, H. Horiuchi, T. Maruyama, and A. Ohnishi, Prog. Theor. Phys. **87**, 1185 (1992).
[25] Y. Kanada-En'yo, M. Kimura, and H. Horiuchi, C. R. Phys. **4**, 497 (2003).
[26] T. Ando, K. Ikeda, and A. Tohsaki, Prog. Theor. Phys. **64**, 1608 (1980).
[27] N. Yamaguchi, T. Kasahara, S. Nagata, and Y. Akaishi, Prog. Theor. Phys. **62**, 1018 (1979); R. Tamagaki, *ibid*. **39**, 91 (1968).
[28] M. W. Kirson, Nucl. Phys. **A301**, 93 (1978).
[29] P. Ring and P. Schuck, *The Nuclear Many-Body Problem* (Springer-Verlag, New York, 1980).
[30] R. E. Pywell, B. L. Berman, J. G. Woodworth, J. W. Jury, K. G. McNeill, and M. N. Thompson, Phys. Rev. C **32**, 384 (1985).
[31] J. G. Woodworth, K. G. McNeill, J. W. Jury, R. A. Alvarez, B. L. Berman, D. D. Faul, and P. Meyer, Phys. Rev. C **19**, 1667 (1979).
[32] S. C. Fults, J. T. Caldwell, B. L. Berman, R. L. Bramblett, and R. R. Harvey, Phys. Rev. **143**, 790 (1966).
[33] B. L. Berman, D. D. Faul, R. A. Alvarez, and P. Meyer, Phys. Rev. Lett. **36**, 1441 (1976).
[34] M. Kimura, Y. Sugawa, and H. Horiuchi, Prog. Theor. Phys. **106**, 115 (2001).
[35] Y. Alhassid, M. Gai, and G. F. Bertsch, Phys. Rev. Lett. **49**, 1482 (1982).
[36] H. Sagawa and M. Honma, Phys. Lett. **B251**, 17 (1990).
[37] N. Imai *et al*., Phys. Rev. Lett. **92**, 062501 (2004).
[38] Z. Elekes *et al*., Phys. Lett. **B586**, 34 (2004).
[39] H. Sagawa, X. R. Zhou, and X. Z. Zhang and T. Suzuki, Phys. Rev. C **70**, 054316 (2004).
[40] M. Takashina, Y. Kanada-En'yo, and Y. Sakuragi, Phys. Rev. C **71**, 054602 (2005).
[41] Y. Kanada-En'yo, Phys. Rev. Lett. **81**, 5291 (1998).
[42] N. Itagaki and S. Aoyama, Phys. Rev. C **61**, 024303 (2000).
[43] G. Thiamova, N. Itagaki, T. Otsuka, and K. Ikeda, Nucl. Phys. **A719**, 312c (2003).